

# Global Energetics of Solar Flares: X. Petschek Reconnection Rate and Alfvén Mach Number of Magnetic Reconnection Outflows

Markus J. Aschwanden

*Solar and Astrophysics Laboratory, Lockheed Martin Advanced Technology Center, Dept. ADBS, Bldg.252, 3251 Hanover St., Palo Alto, CA 94304, USA; (e-mail: [aschwanden@lmsal.com](mailto:aschwanden@lmsal.com))*

## ABSTRACT

We investigate physical scaling laws for magnetic energy dissipation in solar flares, in the framework of the Sweet-Parker model and the Petschek model. We find that the total dissipated magnetic energy  $E_{diss}$  in a flare depends on the mean magnetic field component  $B_f$  associated with the free energy  $E_f$ , the length scale  $L$  of the magnetic area, the hydrostatic density scale height  $\lambda$  of the solar corona, the Alfvén Mach number  $M_A = v_1/v_A$  (the ratio of the inflow speed  $v_1$  to the Alfvénic outflow speed  $v_A$ ), and the flare duration  $\tau_f$ , i.e.,  $E_{diss} = (1/4\pi)B_f^2 L \lambda v_A M_A \tau_f$ , where the Alfvén speed depends on the nonpotential field strength  $B_{np}$  and the mean electron density  $n_e$  in the reconnection outflow. Using MDI/SDO and AIA/SDO observations and 3-D magnetic field solutions obtained with the vertical-current approximation nonlinear force-free field code (VCA-NLFFF) we measure all physical parameters necessary to test scaling laws, which represents a new method to measure Alfvén Mach numbers  $M_A$ , the reconnection rate, and the total free energy dissipated in solar flares.

*Subject headings:* Sun: Flares — Sun: Magnetic Fields — Sun: Corona

## 1. INTRODUCTION

Key observations that provide evidence for magnetic reconnection in solar flares have been furnished mostly from Yohkoh observations: (i) the X-point geometry that is visible as cusp in long-duration events (Tsuneta et al. 1992); (ii) the altitude of the X-point as observed in above-the-loop-top hard X-ray sources (Masuda et al. 1994) and with time-of-flight measurements (Aschwanden et al. 1996); (iii) the rise of the X-point with time that maps to separating footpoints and double ribbons (Sakao et al. 1998; Fletcher and Hudson 2001); (iv) the horizontal symmetry as observed in simultaneous hard X-ray emissions from conjugate footpoints (Sakao 1994); (v) the vertical symmetry as observed in bi-directional type III bursts (Aschwanden et al. 1995), in correlations between hard X-ray pulses and type III bursts (Aschwanden et al. 1993), and in vertically symmetric hard X-ray sources below and above the X-point (Sui and Holman 2003); (vi) post-reconnection relaxation measured from the loop shrinking ratio (Forbes and Acton 1996) and the progression of cooling loops below hot loops (Svestka et al. 1987); (vii) reconnection inflows detected as inward motion in EUV emission (Yokoyama et al. 2001); (viii) reconnection outflows observed as supra-arcade downflows (McKenzie and Hudson 1999); (ix) slow-mode standing shocks in high-temperature ridges of the flare arcade (Tsuneta 1996); and (x) fast-mode standing shocks indicated by high densities above looptops (Tsuneta 1997b) and by above-the-loop-top hard X-ray sources (Masuda et al. 1994). Most of these observations are consistent with the standard flare scenario of Carmichael (1964), Sturrock (1966), Hirayama (1974), Kopp and Pneuman (1976), Tsuneta (1996; 1997a; 1997b), and Shibata et al. (1995), also known as CSHKP model (named after the initials of the first five authors).

While most of the previously listed key observations capture the ongoing physics in solar flare magnetic reconnection processes in a qualitative way, based on 2-D images in soft X-rays and EUV, more quantitative models can be established by physical scaling laws. A first step is the evaluation of which physical parameters are relevant for the derivation of a scaling law, and the second step involves fitting theoretical scaling laws to observations. A compilation of scaling laws for coronal heating processes has been pioneered in Mandrini et al. (2000), which are also applicable to solar flare heating processes. Their study includes a variety of 22 theoretical scaling laws of the power law form  $\varepsilon \propto B^a L^b \rho^c v^d R_c$ , with  $\varepsilon$  the volumetric heating rate,  $B$  the average coronal field strength,  $L$  a length scale of loops,  $\rho$  the mass density,  $v$  the transverse velocity at the chromospheric footpoints, and  $R_c$  a characteristic horizontal length scale for the magnetic field or flow. The application of these scaling laws to observations in Mandrini et al. (2000), however, has some shortcomings: (i) the mean magnetic field  $B$  is parameterized as a function of the loop length  $L$ , i.e.,  $B(L) \propto L^\delta$ , but the power law slope  $\delta$  differs for small loops (in the near-field zone) and large loops (in the far-field zone), and thus invalidates their power law "ansatz"; (ii) The magnetic field component  $B$  is measured from potential and non-potential force-free field extrapolations, but ignores the fact that only the free (magnetic) energy can be dissipated into other forms of energy in coronal heating or flare events; and (iii) other physical parameters that turn out to be important for a realistic scaling law are ignored, such as the magnetic field associated with the free energy ( $B_f \propto \sqrt{E_f}$ ), the Alfvén speed in the reconnection outflows ( $v_A$ ), the reconnection inflow speed ( $v_1 = v_A M_A$ ), the Alfvén Mach number ( $M_A$ ), or the hydrostatic electron density scale height ( $\lambda$ ). Although the starting point of the study of Mandrini et al. (2000) deals with non-flaring loop heating, rather than solar flare processes that are the focus of this study, both phenomena are produced by magnetic reconnection processes, and thus can be quantified with the same scaling laws. We will address more comprehensive scaling laws for magnetic reconnection in solar flares in this study that improve on these shortcomings.

What is the progress in modeling physical scaling laws of magnetic reconnection processes in solar flares, compared with the observational highlights during the Yohkoh mission? Modeling of the 3-D geometry of the space-filling magnetic field  $\mathbf{B} = [B_x(x, y, z), B_y(x, y, z), B_z(x, y, z)]$ , which beyond the potential field, calculates force-free field solutions of the nonpotential field and the free energy, containing the only amount that can be dissipated in solar flares, have become available in the recent decade only. In this study, based on the data analysis from Paper I and Paper IX, magnetic parameters have been computed with the *Vertical-Current Approximation Non-Linear Force-Free Field (VCA-NLFFF)* code, which determines the free energy from the current-driven helical twisting of magnetic field lines. Typically, the azimuthally twisted magnetic field component  $\mathbf{B}_f = \mathbf{B}_\varphi$  is a factor of  $B_f/B_{np} \approx 0.3 \pm 0.1$  smaller than the co-spatial nonpotential field strength, which implies that the free energy is by a factor of  $E_f/E_{np} \approx 0.10 \pm 0.07$  smaller. Thus the discrimination of nonpotential and free energy is important in the energy budget of solar flares. On the other hand, the Alfvén velocity  $v_A$  has to be computed based on the (total) nonpotential magnetic field strength  $B_{np}$ , rather than on the azimuthally twisted field component  $B_f$  that is associated with the free energy.

In this study we address mostly the Sweet-Parker model and the Petschek model applied to solar flares, but there are also applications of Petschek-type reconnection to the magnetopause and solar wind, dealing with unsteady Petschek reconnection (Biernat et al. 1987), resistivity enhancement by instabilities (Kulsrud 2001), current-driven anomalous resistivity (Uzdensky 2003; Büchner 2006), or Petschek-type reconnection exhausts in the solar wind (Gosling et al. 2006a, 2006b).

The content of this paper includes a theoretical description of the Sweet-Parker current sheet model and the Petschek model (Section 2), observations and data analysis of M- and X-class solar flare events (Section

3), a discussion of observational evidence for reconnection inflows, the Alfvén Mach number, flare ribbon motions, and scaling law parameterization (Section 4), and conclusions (Section 5).

## 2. THEORY OF SCALING LAWS

In the following sections we define theoretical scaling laws that quantify the volumetric energy dissipation rate  $\varepsilon_{diss}$  (in units of  $[\text{erg cm}^{-3} \text{ s}^{-1}]$ ) as a function of physical parameters measured during flare events, such as the coronal mean nonpotential magnetic field strength  $B_{np}$ , the magnetic field component  $B_f$  associated with the free energy, the length scale  $L$  of the magnetic field (fractal) area, and the electron density  $n_e$ . The free energy component is generally defined by the difference between the nonpotential and potential field component, which can be represented by a vector difference equation,  $\mathbf{B}_f = \mathbf{B}_{np} - \mathbf{B}_p$ , or by an energy difference equation,  $B_f^2 = B_{np}^2 - B_p^2$ , and quantifies the maximum energy that can be dissipated during a flare. We define the volumetric energy dissipation rate  $\varepsilon_{diss}$  by

$$\varepsilon_{diss} \propto L^a B_{np}^b B_f^c n_e^d \quad [\text{erg cm}^{-3} \text{ s}^{-1}] , \quad (1)$$

in the form of power law dependencies (with power exponents  $a, b, c, d$ ). Since we are interested in the total energy dissipated in a flare event, we have to integrate the volumetric dissipation rate  $\varepsilon_{diss}$  (in units of  $[\text{erg cm}^{-3} \text{ s}^{-1}]$ ) over the flare volume  $V$  and flare duration  $\tau_f$ ,

$$E_{diss} = \varepsilon_{diss} V \tau_f \quad [\text{erg}] . \quad (2)$$

We characterize the scaling of the flare volume  $V$  as a function of the length scale  $L$  with the Euclidean 3-D dimension,

$$V(L) = L^3 \quad [\text{cm}^3] . \quad (3)$$

With these definitions (Eqs. 1-3), the total dissipated energy  $E_{diss}$  can be expressed as

$$E_{diss} \propto L^{(a+3)} B_{np}^b B_f^c n_e^d \tau_f \quad [\text{erg}] . \quad (4)$$

Note that the scaling laws are different for the two energy parameters  $\varepsilon_{diss}$  and  $E_{diss}$ , due to the length dependence of the flare volume  $V(L)$ . For completeness we define also the Poynting flux  $P$ , which is defined by the energy input rate or dissipation rate per unit area,

$$P_{diss} = \varepsilon_{diss} L \propto L^{(a+1)} B_{np}^b B_f^c n_e^d \quad [\text{erg cm}^{-2} \text{ s}^{-1}] . \quad (5)$$

### 2.1. The Sweet-Parker Current Sheet

One of the first theoretical concepts of a magnetic reconnection process occurring in a solar flare is the so-called Sweet-Parker current sheet (Sweet 1958; Parker 1963, 1988). The theoretical derivation of this process can be found in recent textbooks (e.g., p.120 in Priest and Forbes 2000; p.409 in Aschwanden 2004). A main assumption is that the diffusion region is much longer than wide,  $\Delta \gg \delta$  (Fig. 1, left). For steady, compressible flows ( $\nabla \cdot \mathbf{v} \neq 0$ ), it was found that the reconnection outflow  $v_2$  roughly has Alfvén speed,

$$v_2 \approx v_A = \frac{B_2}{\sqrt{4\pi m_p n_e}} , \quad (6)$$

Observationally, the outflow speed  $v_2$  is slower than the expected Alfvén velocity  $v_A$ . Since the Alfvén speed scales reciprocally with the square root of the electron density,  $v_A \propto \sqrt{n_e}$ , a lower value of  $v_A$  could

be explained by larger electron densities  $n_E$  in flaring reconnection regions. The outflow speed  $v_2$  relates to the inflow speed  $v_1$  reciprocally to the cross sections  $\delta$  and  $\Delta$  and mass densities  $\rho_1 = m_p n_1$  and  $\rho_2 = m_p n_2$  (according to the continuity equation),

$$\rho_1 v_1 \Delta = \rho_2 v_2 \delta, \quad (7)$$

and that the *reconnection rate*  $M_A$ , defined as the Mach number ratio of the external inflow speed  $v_1$  to the (Alfvén) outflow speed  $v_A$ , is

$$M_A = \frac{v_1}{v_A} = \frac{1}{\sqrt{S}}. \quad (8)$$

The *Lundquist number*  $S$  (or *magnetic Reynolds number*  $R_m$ ) is defined by

$$S = v_A L / \eta, \quad (9)$$

analogous to the Reynolds number  $R = vL/\eta$  defined for a general fluid velocity  $v$ .

So, for typical coronal conditions (with a large Lundquist number of  $S = R_m \approx 10^8 - 10^{12}$ ) the reconnection rate is typically  $M_A \approx 10^{-4} - 10^{-6}$ , which yields inflow speeds in the order of  $v_1 \approx v_A M_A \approx 1000 \text{ km s}^{-1} \times 10^{-5} \approx 0.1 \text{ km s}^{-1}$  and predicts extremely thin current sheets with a thickness of  $\delta = \Delta(v_1/v_A) \approx \Delta \times 10^{-5}$ . So, a current sheet with a length of  $\Delta \approx 10,000 \text{ km}$  would have a thickness of only  $\delta \approx 0.1 \text{ km}$ . The predicted total energy  $E_{diss}$  dissipated during a flare with duration  $\tau_f$  is (with the label MR1 denoting the first type of magnetic reconnection model),

$$E_{MR1} = \int \left( \frac{dE}{dt} \right) dt \approx 2 \frac{B_f^2}{8\pi} \frac{dV}{dt} \tau_f \approx \frac{B_f^2}{4\pi} L^2 v_1 \tau_f \approx \frac{1}{4\pi} B_f^2 L^2 v_A M_A \tau_f. \quad (10)$$

The term  $dV/dt = L^2 v_1$  describes the inflow rate of the plasma volume into the reconnecting diffusion region (Fig. 1 top). The factor 2 accounts for the symmetric plasma inflows on both sides of a vertical current sheet. The volume is normalized to an Euclidean 3-D cube with length scale  $L$  and filling factor of unity, i.e.,  $V = L^3$  (Eq. 3).

The mean volumetric heating rate  $\varepsilon$  is defined by dividing the total dissipated energy by the flare volume  $V$  and by the flare duration  $\tau_f$  (Eq. 2), which yields a scaling law of

$$\varepsilon_{MR1} = \frac{E_{MR1}}{V \tau_f} = \frac{E_{MR1}}{L^3 \tau_f} = \frac{1}{4\pi} B_f^2 L^{-1} v_A M_A. \quad (11)$$

For typical solar flares parameters, which we take from the median values of the parameter set analyzed in the following Section and listed in Table 1, ( $B_{np} = 240 \text{ G}$ ,  $B_f = 70 \text{ G}$ ,  $L = 3.4 \times 10^9 \text{ cm}$ ,  $n_e = 9 \times 10^{10} \text{ cm}^{-3}$ ,  $\tau_f = 900 \text{ s}$ ,  $S = 10^{10}$ , we obtain (with Eq. 10) typical values of  $M_A = 1/\sqrt{S} = 10^{-5}$  for the Alfvén Mach number,  $v_A = 1700 \text{ km s}^{-1}$  for the Alfvén speed,  $E_{diss} \approx 7 \times 10^{27} \text{ erg}$  for the total dissipated energy, and (with Eq. 11) a volumetric energy dissipation rate of  $\varepsilon_{diss} \approx 2 \times 10^{-4} \text{ erg cm}^{-3} \text{ s}^{-1}$ , which corresponds to a Poynting flux of  $P = \varepsilon_{diss} L \approx 7 \times 10^5 \text{ erg cm}^{-2} \text{ s}^{-1}$ .

Alternatively we can insert the explicit definition of the Alfvén velocity (Eq. 5),  $v_A = B_{np}/\sqrt{4\pi m_p n_e} \approx 2 \times 10^{11} B_{np} n_e^{-1/2}$ , which yields a modified scaling law of

$$E_{MR2} \approx \frac{1}{4\pi \sqrt{4\pi m_p}} B_f^2 B_{np} L^2 n_e^{-1/2} M_A \tau_f. \quad (12)$$

and a modified energy dissipation rate of

$$\varepsilon_{MR2} = \frac{E_{MR2}}{V \tau_f} = \frac{E_{MR2}}{L^3 \tau_f} \approx \frac{1}{4\pi \sqrt{4\pi m_p}} B_f^2 B_{np} L^{-1} n_e^{-1/2} M_A \tau_f. \quad (13)$$

For both models ( $E_{MR1}$  and  $E_{MR2}$ ), the obtained dissipated energies are much smaller than typical flare energies, found to be in the range of  $E_f \approx 10^{28} - 10^{32}$  (Crosby et al. 1993). Consequently, the Sweet-Parker reconnection rate is much too slow to explain the magnetic dissipation in solar flare events. However, such small dissipated energies have been employed in the interpretation of (undetected) nanoflares (Parker 1983) and of (detected) smallest extreme-ultraviolet (EUV) flare-like brightenings (Benz and Krucker 1999; Parnell and Jupp 2000; Aschwanden et al. 2000), in the energy range of  $E_f \approx 10^{24} - 10^{26}$  erg.

## 2.2. Petschek Model

A much faster reconnection model was proposed by Petschek (1964), which involved reducing the size of the diffusion region to a very compact area ( $\Delta \approx \delta$ ) that is much shorter than the Sweet–Parker current sheet ( $\Delta \gg \delta$ ) (Fig. 1, right panel). While the original (2-D) version of the Sweet-Parker model envisions a single large vertical current sheet located above a flare arcade (Fig. 2, left panel), the original Petschek model encompasses a much smaller current sheet with the 2-D geometry of an X-point. However, more realistic (3-D) models of the Petschek-type that account for sufficient reconnection flux invoke many small-scale current sheets that are formed by the tearing mode in coalescing magnetic islands with magnetic O-points and X-points (Fig. 2, right panel; Aschwanden 2002 and references therein).

Summaries of the Petschek model can be found in Priest (1982, p. 351), Jardine (1991), Priest & Forbes (2000, p. 130), Treumann & Baumjohann (1997, p. 148), and Tajima & Shibata (2002, p. 225). Because the length of the current sheet is much shorter, the propagation time through the diffusion region is shorter and the reconnection process becomes faster. However, in a given external area with size  $L_e$  comparable with the length  $\Delta$  of the Sweet–Parker current sheet, a much smaller fraction of the plasma flows through the Petschek diffusion region with size  $\Delta_P$ , where finite resistivity  $\sigma$  exists and field lines reconnect. Most of the inflowing plasma turns around outside the small diffusion region and *slow-mode shocks* arise where the abrupt flow speed changes from  $v_1$  to  $v_2 = v_A$  in the outflow region (Fig. 1, bottom panel). The shock waves represent an obstacle in the flow and thus are the main sites where inflowing magnetic energy is converted into heat and kinetic energy. Simple energy considerations show that inflowing kinetic energy is split up roughly in equal parts into kinetic and thermal energy in the outflowing plasma (Priest & Forbes 2000). Petschek (1964) estimated the maximum flow speed  $v_e$  by assuming a magnetic potential field in the inflow region and found that at large distance  $L_e$  the external field  $B_0(L_e)$  scales logarithmically with distance  $L_e$ ,

$$B_0(L_e) = B_0 \left[ 1 - \frac{4M_A}{\pi} \ln \left( \frac{L_e}{\Delta} \right) \right] . \quad (14)$$

Petschek (1964) estimated the maximum reconnection rate  $M_A$  at a distance  $L_e$  where the internal magnetic field is half of the external value (i.e.,  $B_0(L_e) = B_0/2$ ), which yields using Eq. (14),

$$M_A = \frac{\pi}{8 \ln(L_e/\Delta)} \approx \frac{\pi}{8 \ln(R_{me})} . \quad (15)$$

So, the reconnection rate  $M_A = v_1/v_A$  depends only logarithmically on the magnetic Reynolds number  $R_{me} = L_e v_{Ae}/\eta$ . Therefore, for coronal conditions, where the magnetic Reynolds number is very high (i.e.,  $R_{me} \approx 10^8 - 10^{12}$ ), the Petschek reconnection rate is  $M_A \approx 0.01 - 0.02$  according to Eq. (15), yielding an inflow speed of  $v_1 \approx v_A$   $M_A \approx 10 - 20$  km s<sup>-1</sup> for typical coronal Alfvén speeds of  $v_A \approx 1000$  km s<sup>-1</sup>. Thus, the Petschek reconnection rate is about three orders of magnitude faster than the Sweet–Parker reconnection rate. The Petschek model can be expressed with the same formal scaling laws as the Sweet-Parker current

sheet (Eq. 10 and 11), except for the expression of the Alfvénic Mach number (Eq. 15), which is substantially higher than in the Sweet-Parker current sheet model (Eq. 8).

MHD (hybrid) simulations have shown that magnetic reconnection remains Alfvénic in a collisionless system even for very large macroscopic scale lengths, yielding a universal constant for the reconnection rate with an inflow velocity towards the X-line around  $v_1 \approx 0.1 v_A$ , which implies a Mach number of  $M_A = 0.1$  (Shay et al. 1999).

The canonical volume definition  $V(L) = L^3$  is subject to the hydrostatic density structure of the solar corona, which can introduce a hydrostatic weighting bias in coronal temperature measurements (Aschwanden and Nitta 2000). Since the vertical electron mass density approximately follows an exponential function with a scale height  $\lambda(T_e)$  that depends linearly on the temperature  $T_e$ , the volume of the diffusion region  $V_\lambda$  in a vertical current sheet can be modeled with a square area  $A$  and a vertical scale height  $\lambda$ ,

$$V_\lambda(T) = A\lambda = L^2 \lambda, \quad \lambda \approx 5 \times 10^9 \left( \frac{T_e}{1 \text{ MK}} \right) [\text{cm}], \quad (16)$$

which also affects the scaling laws. Therefore, the model MR1 (Eq. 10) is modified to

$$E_{MR3} = \int \left( \frac{dE}{dt} \right) dt \approx \frac{B_f^2}{4\pi} L \lambda v_1 \tau_f \approx \frac{1}{4\pi} B_f^2 L \lambda v_A M_A \tau_f, \quad (17)$$

and similarly model MR2 (Eq. 12) is modified to

$$E_{MR4} \approx \frac{1}{4\pi \sqrt{4\pi m_p}} B_f^2 B_{np} L n_e^{-1/2} \lambda M_A \tau_f. \quad (18)$$

Thus we specified four different versions of Petschek models, i.e., MR1 (Eq. 10), MR2 (Eq. 12), MR3 (Eq. 17), MR4 (Eq. 18), which differ from each other in the assumptions made in the Alfvén velocity measurements ( $v_A = \text{const}$  versus  $v_A \propto B_f/\sqrt{n_e}$ ) or different volume scaling laws ( $V \propto L^3$  versus  $V \propto L^2\lambda$ ).

### 3. OBSERVATIONAL DATA ANALYSIS

#### 3.1. Observations

We use the same data set of 173 solar flares presented in Paper I (Aschwanden et al. 2014) and Paper II (Aschwanden et al. 2015), which includes all M- and X-class flares observed with the SDO (Pesnell et al. 2011) during the first 3.5 years of the mission (2010 June 1 to 2014 January 31). Eliminating of data gaps or outliers leaves us with 167 events (or 162 correlations) for further analysis. This selection of events has a heliographic longitude range of  $[-45^\circ, +45^\circ]$ , for which magnetic field modeling can be facilitated without too severe foreshortening effects near the solar limb. We use the 45-s line-of-sight magnetograms from HMI/SDO and make use of all coronal EUV channels of AIA (Lemen et al. 2012) onboard the *Solar Dynamics Observatory* (SDO) (in the six wavelengths 94, 131, 171, 193, 211, 335 Å), which are sensitive to strong iron lines in the temperature range of  $T \approx 0.6 - 16$  MK. The spatial resolution is  $\approx 1.6''$  (0.6'' pixels) for AIA, and the pixel size of HMI is  $0.5''$ . The coronal magnetic field is modeled by using the line-of-sight magnetogram  $B_z(x, y)$  from the *Helioseismic and Magnetic Imager* (HMI) (Scherrer et al. 2012) and (automatically detected) projected loop coordinates  $[x(s), y(s)]$  in each EUV wavelength of AIA. A full 3-D magnetic field model  $\mathbf{B}(x, y, z)$  is computed for each time interval and flare with a cadence of 6 min, where the total duration of a flare is defined by the GOES flare start and end times. The size of the computation

box amounts to an area with a width and length of 0.5 solar radii in the plane-of-sky, and an altitude range of 0.2 solar radius. The total number of analyzed data includes 2706 HMI images and 16,236 AIA images.

For the data analysis of this study, which is focused on the magnetic reconnection rate, we require the following observables: the mean nonpotential magnetic field strength  $B_{np}$ , the mean magnetic field component  $B_f = B_\varphi$  associated with the free energy or azimuthal field component, the spatial length scale  $L$  of the magnetic area in the flare region, the mean electron density  $n_e$ , the flare duration  $\tau_f$ , the free energy  $E_f$ , and the total dissipated magnetic energy  $E_{diss}$  during the flare duration.

The magnetic parameters  $B_{np}$ ,  $B_\varphi$ ,  $E_f$ ,  $E_{diss}$  are all computed with the *Vertical-Current Approximation Nonlinear Force-Free Field (VCA-NLFFF)* code, as described in Paper I and Paper IX. This magnetic field extrapolation code essentially assumes vertical currents at flare locations that are associated with sub-photospheric magnetic field concentrations (e.g., sunspots and smaller magnetic features). A major advantage of this code over traditional NLFFF codes is the capability to measure the current-driven twisting of coronal magnetic field lines, based on automated tracing of coronal loops in AIA images, which this way bypasses the non-force-freeness of the photospheric field.

The spatial scale  $L$  is measured from the area  $A = L^2$  of the (time-accumulated) azimuthal magnetic field, i.e.,  $B_\varphi(x, y) \geq 100$  G, after correction of projection effects (Paper I). The electron density  $n_e$  is obtained from a *differential emission measure (DEM)* analysis, using the relationship of the total emission measure  $EM$  with the electron density, i.e.,  $EM = n_e^2 V \approx n_e^2 L^3$  (Paper II). The quantities  $B_\varphi$ ,  $L$ ,  $n_e$  are determined at the peak times of the flare emission measure, while the parameters  $E_f$  and  $E_{diss}$  are integrated over the flare duration  $\tau$ . The minimum, maximum, mean and standard deviation, and median values are listed in Table 1 and histogrammed in Fig. 3.

### 3.2. Magnetic Reconnection Scaling Law Tests

The total dissipated energy  $E_{diss}$  in a flare is a fundamental parameter, for which a scaling law has been considered in terms of the Sweet-Parker model (Section 2.1) and the Petschek model (Section 2.2), according to Eq. (10), where an Alfvén Mach number of  $M_A \approx 10^{-5}$  is typical for the Sweet-Parker model (Eq. 8), and a value of  $M_A \approx 10^{-1}$  for the Petschek model (Eq. 15). We plot the theoretically predicted magnetic dissipation energies  $E_{MR1}^{pred}$  of the first model (Eq. 10) as a function of the observed dissipation energies  $E_{MR1}^{diss}$  in Fig. 4a. The theoretical model is obviously related to the observed values. We measure three different criteria to quantify this relationship: (i) the cross-correlation coefficient

$$CCC = \frac{\sum_i E_{pred} E_{diss}}{\sum_i E_{pred} \times \sum_i E_{diss}}, \quad (19)$$

between the observed  $E_{diss}$  and the scaling-law predicted theoretical values  $E_{pred}$ ; (ii) the slope  $p$  of the linear regression fit; and (iii) the median energy ratio  $q_E = E_{pred}/E_{obs}$ . These three criteria have the values of  $CCC = 0.79$ ,  $p = 1.35$ , and  $q_E = 0.68$  for model MR1 (Fig. 4a), so it indicates a positive correlation, but does not match exactly the linear regression slope  $p$  and median energy ratio  $q_E$ .

In model MR2 (Fig. 4b) we use the actually observed values  $B_{np}$  and  $n_e$  in the calculation of the Alfvén speed, while we used the constant value  $v_A = 1700$  km s $^{-1}$  in model [MR1], which is the median value of all events. The results are not much different in the second model (MR2), except for a worse linear regression slope of  $p = 1.52$ , likely to be caused by uncertainties of the parameters  $B_{np}$  and  $n_e$ .

In the models MR3 (Fig. 4c) and MR4 (Fig. 4d) we use the hydrostatic volume scaling  $V = L^2 \lambda$ , in

contrast to the standard volume cubes  $V = L^3$  used in the first two models (MR1, MR2). Interestingly, the linear regression slope  $p$  improves to a value of  $p = 1.07$ , which is close to the theoretically expected value  $p = 1.0$  in the case of a matching scaling law. Apparently, consideration of the hydrostatic scale height is a necessary ingredient to improve the empirical scaling law for magnetic reconnection, which has been ignored in previous studies.

What do these results tell us? If we accept the model MR3 as the best match to a magnetic reconnection model, we learn (i) that the high cross-correlation coefficient of  $CCC = 0.73$  implies that the underlying scaling law  $E_{diss} \propto B_f^2 L v_A$  (Eq. 17) renders the most likely functional relationship, (ii) that an Alfvén Mach number of  $M_A \approx 0.1$  predicts the correct magnitude of an energy dissipation event, and (iii) that the hydrostatic scaling of the diffusion region has to be taken into account to obtain accurate mean electron densities.

As a caveat, we have to consider the ambiguity of the values in the product  $\lambda M_A$  (Eq. 17) in the scaling law of model MR3. The exponential electron density scale height scales linearly with the temperature,  $\lambda \propto T_e$ , which is not explicitly measured here. The Alfvén Mach number  $M_A$  is another parameter that is not known in our data set. Thus, the product of these two quantities is ambiguous. In the models MR1-MR4 discussed here we assumed a coronal temperature of  $T_e = 1.0$  MK and a Mach number of  $M_A = 0.1$ . Theoretically, a reciprocal choice of  $T_e = 2.0$  MK and  $M_A = 0.05$  would yield an identical product. However, it has been argued that the inflows into the diffusion region of a magnetic reconnection process are expected to be of coronal temperatures ( $T_e \approx 1 - 2$  MK), rather than of flare plasma temperatures ( $T_e \approx 5 - 25$  MK), because the flowing plasma would be supplied from the corona surrounding the flare (Hara and Ichimoto 1996).

### 3.3. Alfvén Mach Number

Adopting the best-fitting model MR3 (Eq. 17) we obtain a simple expression for inferring the Alfvén Mach Number  $M_A$  from the observables  $(B_f, L, \lambda, v_A, \tau_f)$ ,

$$M_A = \frac{4\pi E_{diss}}{B_f^2 L \lambda v_A \tau_f}, \quad (20)$$

where the mean free energy field strength  $B_f = B_\varphi$  and dissipated energy  $E_{diss}$  are obtained from the nonlinear force-free field solution  $\mathbf{B}_f$  averaged over the volume of the computation box,  $L = \sqrt{A}$  is the length scale obtained from the magnetic flare area  $A$  above some threshold (e.g.,  $B > 100$  G),  $v_A = B_{np}/\sqrt{4\pi m_p n_e}$  is the Alfvén velocity measured in the reconnection outflow, given by the mean nonpotential force-free solution  $\mathbf{B}_{np}$ , the electron density  $n_e$  in the reconnection outflow, and the flare duration  $\tau_f$ , for instance from the GOES flare start and end time. We show the results of the so obtained Alfvén Mach numbers  $M_A$  in Fig. 5, juxtaposed to other previous measurements. Note that most observational results of Mach numbers were inferred from velocity measurements of reconnection inflows or outflows (e.g., with Yohkoh/SXT), rather than from nonlinear force-free field solutions as done here. In this sense we offer a new method to determine the Alfvén Mach number, based on observations of the magnetic field (HMI/SDO) and EUV images (AIA/SDO).

The Alfvénic Mach number is defined as  $M_A = v_1/v_A$ , where the Alfvén speed is defined by  $v_A = B_f/\sqrt{\mu_0 n_e}$ , with  $B_f$  the mean magnetic energy in the active region and  $n_e$  the mean electron density. Since the soft X-ray emission measure,  $EM = n_e^2 V$  is a good proxy for the soft X-ray flux  $F_{SXR}$ , we expect that



the Alfvénic Mach number  $M_A$  scales slightly positive with the emission measure or soft X-ray flux, i.e.,  $M_A \propto EM^{1/4} \propto F_{SXR}^{1/4}$ .

## 4. DISCUSSION

### 4.1. Evidence for Magnetic Reconnection Inflows

All magnetic reconnection models require inflows into the sides of the current sheet and predict near-Alfvénic outflows. In solar flares, however, it turned out to be extremely difficult to detect reconnection inflows, either because of low density, low contrast, slow inflow speed, incomplete temperature coverage, or projection effects (Hara and Ichimoto 1996). In the famous “candle-light” flare event observed with Yohkoh/SXT (Soft X-ray Telescope), inflow speeds of  $v_{in} \approx 56 \text{ km s}^{-1}$  ( $M_A \approx 0.07$ ) and outflow speeds of  $v_{out} \approx 800 \text{ km s}^{-1}$  ( $M_A \approx 1$ ) were estimated based on hydrodynamic modeling arguments (Tsuneta (1996). During the Yohkoh era, only one study has been published that shows direct evidence for reconnection inflows in a solar flare, where an inflow speed of  $v_{in} \lesssim 5 \text{ km s}^{-1}$  was measured with EIT/SOHO and a reconnection rate of  $M_A \approx 0.001 - 0.03$  was estimated (Yokoyama et al. 2001), consistent with the range of other estimates,  $M_A \approx 0.001 - 0.01$  (Isobe et al. 2002), see also Fig. 5 for comparisons.

Direct measurements of reconnection outflows are not readily observed either. The first evidence of high-speed downflows above flare loops is believed to be observed by Yohkoh/ SXT during the 1999-Jan-20 flare, showing dark voids flowing down from the cusps, with speeds of  $v_{out} \approx 100 - 200 \text{ km s}^{-1}$  (McKenzie & Hudson 1999; McKenzie 2000), about an order of magnitude slower than expected for coronal Alfvén speeds. The downward outflows hit a high-temperature ( $T \approx 15 - 20 \text{ MK}$ ) region, which might be evidence of the fast-mode shock (Tsuneta 1997a, 1997b), sandwiched between the two ridges of the slow-mode shock (Tsuneta 1996). Blueshifted Fe XXV lines were also interpreted as direct outflows from Petschek-type reconnection regions (Lin et al. 1996).

### 4.2. Alfvén Mach Number

A key parameter to characterize the dynamics and geometry of the diffusion region of a magnetic reconnection process is the Alfvén Mach number  $M_A$ , which is the ratio of the sideward inflow velocity  $v_1$  to the vertical outflow speed  $v_2$  (Eq. 8). In the Sweet-Parker model (Sweet 1958; Parker 1963), a very low value of  $M_A = 1/\sqrt{S} \approx 10^{-5}$  was adopted, due to the high value of the Lundquist number  $S \approx 10^{10}$  adopted for the solar corona. Petschek (1964) derived a much higher value of  $M_A \approx 0.01 - 0.02$ , due to the logarithmic dependence on the Reynolds number. Further theoretical studies that include the external region for Petschek’s mechanism in greater detail revealed upper limits at approximately 20% of Petschek’s value (Roberts and Priest 1975). This trend continued with numerical MHD simulations, leading to high values of up to  $M_A \approx 0.1$  (Shay et al. 1999). For a juxtaposition of different Alfvén Mach numbers see Fig. 5. The Petschek’s reconnection mechanism is considered to be a particular solution of the MHD equations that apply only when special conditions are met (Forbes 2001). Alternatively to MHD simulations, two-fluid concepts were employed, where ions and electrons have different temperatures, which splits the reconnection outflow into multiple streaming channels (Longcope and Bradshaw 2010).

### 4.3. Flare Ribbon Motion

Magnetic reconnection is often modeled as a quasi-stationary steady-state scenario, operating in an equilibrium between lateral inflows into a vertical current sheet, and reconnection outflows in upward and downward direction. There is also evidence for dynamic time evolution, where the footpoint ribbons systematically move apart, while the centroid of the magnetic reconnection X-point rises upward, as a consequence of the self-similar reconnection geometry. Such separation motion of soft X-ray and EUV flare ribbons have been observed in many flares (e.g., Tsuneta et al. 1992; Fletcher and Hudson 2001; Krucker et al. 2003; Asai et al. 2004; Sui et al. 2004; Veronig et al. 2006; Vrsnak et al. 2006; Temmer et al. 2007). Another dynamics of flare ribbons is the elongation motion along the polarity inversion line (Qiu et al. 2017).

The related energy dissipation rate can be written as a product of the Poynting flux into the reconnection region,  $S = B_c v_i / (4\pi)$ , and the area of the reconnection region,  $A$ ,

$$\frac{dE}{dt} = SA = 2 \frac{B_c^2}{4\pi} v_i A = 2 \frac{B_c^2}{4\pi} v_A M_A A, \quad (21)$$

where  $B_c$  is the mean magnetic field strength in the corona, and  $v_i$  is the inflow velocity into the reconnection region (Asai et al. 2004). Strictly speaking, the coronal magnetic field strength should be estimated with the magnetic field component that is associated with the free energy,  $B_c \approx B_f$  (see Eq. 11). Nevertheless, this model predicts a decreasing energy dissipation rate  $E(t)$  when reconnection proceeds to higher altitudes, where  $B_c(t)$  and  $v_i(t)$  decrease with progressive height. More generally, measuring the time-dependent parameters  $[B_f(t), v_A(t), M_A(t)]$  from observations and integrating the time-dependent parameters over the flare duration would lead to more accurate estimates of the flare-dissipated energies, rather than multiplying with the flare duration  $\tau_f$  (as done in Eq. 10).

### 4.4. Scaling Law Parameterization

The long-standing coronal heating problem, which is related to the coronal flare heating problem, has been characterized with scaling laws that involve combinations of physical parameters raised to some power. A variety of 22 different scaling laws of the form  $\varepsilon_{diss} \propto B^a L^b \rho^c v^d R_c$  has been presented in Mandrini et al. (2000), where  $B$  is the average coronal field strength (computed with potential, linear force-free, and magnetostatic extrapolation models),  $L$  a characteristic length scale of coronal loops,  $\rho = m_p n_e$  the mean mass density,  $v$  is the transverse velocity at the base of the corona, and  $R_c$  is a characteristic horizontal length scale for the magnetic field or flow field. Based on a previous study, a universal scaling law of  $\langle B \rangle \propto L^\delta$  with a mean slope of  $\delta = -0.88 \pm 0.3$  has been claimed (Klimchuk and Porter 1995), but the power law slope  $\delta$  was found to be different in the near-field and far-field of a magnetic dipole field, fitting an empirical function of  $\langle B \rangle (L) = c_1 + c_2 \log(L) + C_3/2 \log(L^2 + S^2)$  (Mandrini et al. 2000). Although we deal with the same problem here, our present study differs in a number of assumptions: (i) The dissipated magnetic energy cannot exceed the free energy,  $E_{diss} \leq E_f$ , and thus the associated magnetic field component is  $\mathbf{B}_f = \mathbf{B}_{np} - \mathbf{B}_p$ , rather than the average coronal field strength  $\langle B \rangle = \langle \mathbf{B}_{np} \rangle$  used in Mandrini et al. (2000); (ii) The universal scaling law  $\langle B \rangle \propto L^\delta$  claimed by Klimchuk and Porter (1995) does not hold over the near-field range, and the fitted empirical function (with logarithmic terms) is unphysical; (iii) The electron density scale height  $\lambda$  of the hydrostatic corona is neglected in Mandrini et al. (2000); (iv) Important physical parameters are missing in scaling laws given by Mandrini et al. (2000), which are relevant in most of the included magnetic reconnection scenarios, such as the inflow speed  $v_1$ , the Alfvén speed  $v_A$ , or the Alfvén Mach number  $M_A$ .

A related method to test scaling laws of coronal heating mechanisms was attempted with full-Sun visualizations by Schrijver et al. (2004). Images of the full Sun are simulated in various wavelengths by populating the corona with a total of 50,000 coronal loops, each one characterized with a quasi-static loop top temperature  $T_e$ , footpoint electron density  $n_e$ , and steady-state heating rate  $\varepsilon_{heat}$ . The best match between the observed and simulated soft X-ray and EUV emission of active regions is found for the scaling law of the Poynting flux  $P_{heat} \propto B^{1.0 \pm 0.3} L^{-1.0 \pm 0.5}$  (in units of  $[\text{erg cm}^{-2} \text{ s}^{-1}]$ ), which corresponds to a volumetric heating rate of  $\varepsilon_{diss} \propto P_{heat}/L \propto B^{1.0 \pm 0.3} L^{-2 \pm 1}$ . This result is not consistent with any of our 4 models (MR1: Eq. 10, MR2: Eq. 12, MR3: Eq. 17, MR4: (Eq. 18)). We suspect that similar factors contribute to this discrepancy as discussed above in the study of Mandrini et al. (2000), such as the invalidity of the scaling of  $B \propto L^\delta$ , the proper distinction between the potential, the nonpotential, and free energy in the scaling laws containing the magnetic field  $B$ , as well as the neglect of physical parameters relevant in magnetic reconnection scenarios (inflow speed  $v_1$ , Alfvén speed  $v_A$ , and Alfvén Mach number  $M_A$ ).

While we focused on magnetic scaling laws of flare energies in this study, there exist additional complementary flare scaling laws that involve thermal energies and emission measures (Papers II, V), such as the Rosner-Tucker-Vaiana (Rosner et al. 1978) and the Shibata-Yokoyama scaling law (Shibata and Yokoyama 1999), subject of future studies on heating rates and thermal energies.

## 5. CONCLUSIONS

In this study we focus on testing scaling laws of magnetic flare energies, which is related to magnetic scaling laws responsible for coronal heating, as investigated in previous studies (Mandrini et al. 2000; Schrijver et al. 2004). The most basic magnetic scaling law is the Sweet-Parker model for magnetic reconnection, which has been improved into a more realistic model by Petschek (1964). Although the physical parameters of these theoretical models are well-defined, the application of these scaling laws to observables is not trivial, because of spatio-temporal averaging of flare regions, their restricted observability in 2-D, and the reconstructability of their 3-D geometry. We pursue a new approach with a nonlinear force-free field code that provides the 3-D magnetic structure and quantitative measurements of magnetic parameters, such as the dissipated magnetic energy, the potential, non-potential and free energies, the Alfvén velocity, the reconnection rate, and the Alfvén Mach number. We are using identical data sets as used previously in Paper I and II on the global energetics of flares and CMEs (Aschwanden et al. 2014, 2015), which includes only M-class and X-class flares. In the following we summarize the conclusions of this study:

1. The Sweet-Parker scaling law provides a suitable formalism for the energetics of a basic magnetic reconnection process, but uses an unrealistic Alfvén Mach number based on the high magnetic Reynolds number of order  $S \approx 10^{10}$ , which predicts extremely thin current sheets with widths  $\delta \approx 10^{-5} L$  (that are not stable and would break up due to the tearing mode), and have a too slow reconnection rate to explain solar flares.
2. The Petschek model assumes a potential field in the inflows of the diffusive magnetic reconnection region and finds a logarithmic dependence on the magnetic Reynolds number, which predicts a large reduction in the size of the diffusion region, a much faster reconnection rate (about 3 orders of magnitude faster than the Sweet-Parker model), and an Alfvén Mach number of  $M_A \approx 0.1$  (Fig. 5).
3. For the magnetically dissipated energy  $E_{diss}$  in flares we find a good correlation for the scaling law  $E_{diss} = (1/4\pi)B_f^2 L^2 v_A M_A \tau_f$ , with a cross-correlation coefficient of  $CCC = 0.79$  and a mean energy

ratio of  $q_E = 0.73$ . The median Alfvén velocity is  $v_A = 1700 \text{ km s}^{-1}$  in this model MR1. Inserting the flare-averaged (nonpotential) magnetic field strengths  $B_{np}$  and electron densities  $n_e$  into the expression of the Alfvén velocity  $v_A$ , we find a similar good correlation (in model MR2).

4. Previous estimates of the reconnection inflow rate used a volume scaling of  $V \propto L^3$ , which implies a reconnection outflow rate of  $dV/dt = L^2 v_A$ . Since the electron density distribution of the solar corona is approximately hydrostatic, i.e.,  $n_e(h) \propto e^{-h/\lambda}$ , a volume scaling of  $V \propto L^2 \lambda$  is more realistic, which implies a reconnection outflow rate of  $dV/dt = L \lambda v_A$ . With this hydrostatic correction we obtain a best-fitting model (MR3) that has a cross-correlation coefficient of  $CCC = 0.73$ , a mean energy ratio of  $q_E = 0.96$ , as well as a slope  $p = 1.07$  of the linear regression fit, which is close to the ideal value of  $p = 1.0$  for a perfect match. Since the inflow originates from outside the flare core, the density scale height  $\lambda$  corresponds to the average coronal temperature of  $T_e \approx 1.0 \text{ MK}$ . This optimization changes the scaling law to  $E_{diss} = (1/4\pi) B_f^2 L \lambda v_A M_A \tau_f$ .
5. Measurements of magnetic reconnection inflows have been sparse, due to the low densities, low contrast, low inflow speed, incomplete temperature coverage, or projection effects. Such measurements have been carried out in Yohkoh/SXT data, where the lateral inflow speed was inferred from the spatial displacement of plasma in the cusp regions. Here we present a new method that can corroborate the directly observable projected velocity, or future spectroscopic velocity measurements.
6. There are numerous observations and measurements of flare ribbons, which contain information on the time-dependent energy dissipation  $E_{diss}(t)$  in magnetic reconnection sites, which allows us to study the time evolution of magnetic reconnection processes in flares.
7. Based on the best-fitting magnetic energy scaling law evaluated here, which requires a discrimination between the magnetic free energy  $E_f$  and the nonpotential energy  $E_{np}$ , and of the related magnetic field strengths  $B_f$  and  $B_{np}$ , we conclude that hypothetical scaling laws with a single component  $B$  represent oversimplified approaches that cannot retrieve physically correct scaling laws. Moreover, the scaling  $B(L) \propto L^\delta$  is invalid, because the power law coefficient differs in the near-field and far-field range of a magnetic dipole.

In summary, this study quantifies the scaling law of magnetic reconnection with a number of magnetic parameters ( $B_f, B_{np}, v_A, M_A$ ) that can be used to predict the total magnetic energy  $E_{diss}$  dissipated in solar flares, which provides not only a deeper physical understanding of the underlying magnetic reconnection process, but serves also for statistical predictions of flare energies that are needed in space weather forecasting.

Part of the work was supported by NASA contract NNG 04EA00C of the SDO/AIA instrument and the NASA STEREO mission under NRL contract N00173-02-C-2035.

## REFERENCES

- Asai, A., Yokoyama, T., Shimojo, M., Masuda, S., Kurokawa, H., and Shibata, K. 2004, ApJ 611, 557
- Aschwanden, M.J., Benz, A.O., Dennis, B.R. and Gaizauskas, V. 1993, ApJ 416, 857
- Aschwanden, M.J., Benz, A.O., Dennis, B.R., and Schwartz, R.A. 1995, ApJ 455, 347
- Aschwanden, M.J., Wills, M.J., Hudson, H.S., Kosugi, T., and Schwartz, R.A. 1996, ApJ 468, 398
- Aschwanden, M.J., Tarbell, T., Nightingale, R., Schrijver, C.J., Title, A., Kankelborg, C.C., Martens, P.C.H., and Warren, H.P. 2000, ApJ 535, 1047
- Aschwanden, M.J. and Nitta, N. 2000, ApJ 535, L59
- Aschwanden, M.J. 2002, SSRv 101, 1
- Aschwanden, M.J. 2004, Praxis and Springer, New York, ISBN 3-540-22321-5, First Edition, hardbound issue, 842p Physics of the Solar Corona - An Introduction (1st Edition)
- Aschwanden, M.J., Xu, Y., and Jing, J. 2014, ApJ 797, 50, (Paper I)
- Aschwanden, M.J., Boerner, P., Ryan, D., Caspi, A., McTiernan, J.M., and Warren, H.P. 2015, ApJ 802:53, (Paper II)
- Aschwanden, M.J. 2019, ApJ 885:49, (Paper IX)
- Benz, A.O. and Krucker S., 1999, AA 341, 286
- Biernat, H.K., Heyn, M.F., and Semenov, V.S. 1987, JGR 92/A4, 3392
- Büchner, J. 2006, SSRv 124, 345
- Carmichael, H. 1964, in proc. *The Physics of Solar Flares*, NASA Special Publication 50, (ed. W.N. Hess), NASA, Washington DC, p.451.
- Crosby, N.B., Aschwanden, M.J., and Dennis, B.R. 1993, SoPh 143, 275
- Fletcher, L. and Hudson, H.S. 2001, SoPh 204, 71
- Forbes, T.G. and Acton, L.W. 1996, ApJ 459, 330
- Forbes, T.G. 2001, Earth, Planets and Space 53, 423
- Gosling, J.T., Eriksson, S., Skoug, R.M., McComas, D.J. and Forsyth, R.J. 2006a, ApJ 644, 613
- Gosling, J.T., Eriksson, S., and Schwenn, R. 2006b, JRL, 111, A10, A10102
- Hara, H. and Ichimoto, K. 1996, in Proc. *Magnetic Reconnection in the Solar Atmosphere*, ASP Conf. 111, 183
- Hirayama, T. 1974, SoPh 34, 323
- Isobe, H., Yokoyama, T., Shimojo, M., Morimoto, T., Kozu, H., Eto, S., Narukage, N., and Shibata, K. 2002, ApJ 566, 528
- Jardine, M. 1991, in *Mechanisms of Chromospheric and Coronal Heating*, (eds. P. Ulmschneider, E.R. Priest, and R. Rosner), Springer, Berlin, p.588.

- Klimchuk, J.A. and Porter, L.J. 1995, *Nature*, 377, 131
- Kopp, R.A. and Pneuman, G.W. 1976, *SoPh* 50, 85
- Krucker, S., Hurford, G.J., and Lin, R.P. 2003, *ApJ* 595, L103
- Kulsrud, R.M. 2001, *Earth, Planets and Space* 53, 417
- Lemen, J.R., Title, A.M., Akin, D.J., Boerner, P.F., Chou, C., Drake, J.F., Duncan, D.W., Edwards, C.G., et al. 2012, *SoPh* 275, 17.
- Lin, J., Martin, R., and Wu, N. 1996, *AA* 311, 1015
- Mandrini, C.H., Demoulin, P., and Klimchuk, J.A. 2000, *ApJ* 530, 999
- Masuda, S., Kosugi, T., Hara, H., Tsuneta, S., and Ogawara, Y. 1994 *Nature* 371/6497, 495.
- McKenzie, D.E. and Hudson, H.S. 1999, *ApJ* 519, L93
- McKenzie, D.E. 2000, *SoPh* 195, 381
- Longcope, D.W. and Bradshaw, S.J. 2010, *ApJ* 718, 1491
- Parker, E.N. 1963, *ApJS* 8, 177
- Parker, E.N. 1983, *ApJ* 264, 642
- Parker, E.N. 1988, *ApJ* 330, 474
- Parnell, C.E. and Jupp, P.E. 2000, *ApJ* 529, 554
- Pesnell, W.D., Thompson, B.J., and Chamberlin, P.C. 2011, *SoPh* 275, 3
- Petschek, H.E. 1964, in "The Physics of Solar Flares", *Proc. AAS-NASA Symposium*, (ed. W.N.Hess), Washington DC, p.425
- Priest, E.R. 1982 *Solar Magnetohydrodynamics* Geophysics and Astrophysics Monographs Volume 21, D. Reidel Publishing Company, Dordrecht
- Priest, E.R. and Forbes, T. 2000, Cambridge: Cambridge University Press, *Magnetic reconnection (MHD Theory and Applications)*
- Qiu, J., Longcope, D.W., Cassak, P.A., and Priest, E.R. 2017, *ApJ* 838, 17
- Roberts, B. and Priest, E.R. 1975, *J. Plasma Physics* 14/3, 417
- Rosner, R., Tucker, W.H., and Vaiana, G.S. 1978, *ApJ* 220, 643
- Sakao, T. 1994, PhD Thesis, University of Tokyo
- Sakao, T., Kosugi, T., and Masuda, S. 1998, in *Proc. Observational Plasma Astrophysics: Five Years of Yohkoh and Beyond*, (eds. Watanabe, T., Kosugi, T. and Sterling, A.C.), *Astrophysics and Space Science Library* Vol. 229, p.273-284. Kluwer Academic Publishers, Dordrecht, Netherlands
- Scherrer, P.H., Schou, J., Bush, R.I., Kosovichev, A.G., Bogart, R.S., Hoeksema, J. T., Liu, Y., Duvall, T.L., et al. 2012, *SoPh* 275, 207
- Schrijver, C.J., Sandman, A.W., Aschwanden, M.J., and DeRosa, M.L. 2004, *ApJ* 615, 512

- Shay, M.A., Drake, J.F., Rogers, B.N., and Denton, R.E. 1999, GRL 26, 2163
- Shibata, K., Masuda, S., Shimojo, M., Hara, H., Yokoyama, T., Tsuneta, S., Kosugi, T., and Ogawara, Y. 1995, ApJ 451, L83
- Shibata, K. and Yokoyama, T. 1999, ApJ 526, L49
- Sturrock, P.A. 1966, Nature 5050, 695
- Sui, L. and Holman, G.D. 2003, ApJ 596, L251
- Sui, L., Holman, G.D., and Dennis, B.R. 2004, ApJ 612, 546
- Svestka, Z., Fontenla, J.M., Machado, M.E., Martin, S.F., Neidig, D., Poletto, G. 1987, SoPh 108, 237
- Sweet, P.A. 1958, in "Electromagnetic Phenomena in Cosmic Physics", International Astronomical Union Symposium 6, (ed. B.Lehnert), Cambridge University Press, New York, p.123
- Tajima, T. and Shibata, K. 2002, *Plasma Astrophysics*, Perseus Publishing, Cambridge, Massachusetts
- Temmer, M., Veronig, A.M., Vrsnak, B., and Miklenic, C. 2007, ApJ 654:665
- Treumann, R.A. and Baumjohann, W. 1997, *Advanced space plasma physics*, Imperial College London.
- Tsuneta, S., Hara, H., Shimizu, T., Acton, L.W., Strong, K.T., Hudson, H.S., and Ogawara, Y. 1992, PASJ 44, L63
- Tsuneta, S. 1996, ApJ 456, 840
- Tsuneta, S., Masuda, S., Kosugi, T., and Sato, J. 1997a, ApJ 478, 787
- Tsuneta, S. 1997b, ApJ 483, 507
- Uzdensky, D.A. 2003, ApJ 587:450
- Veronig, A.M., Karlicky, M., Vrsnak, B., Temmer, M., Magdalenic, J., Dennis, B.R., Otruba, W., and Poetzi, W. 2006, AA 446, 675
- Vrsnak, B., Temmer, M., Veronig, A., Karlicky, M., and Lin, J. 2006, SoPh 234, 273
- Yokoyama, T., Akita, K., Morimoto, T., Inoue, K., and Newmark, J. 2001, ApJ 546, L69

Table 1: Observational parameters of  $N = 162$  M- and X-class flare events analyzed in Aschwanden, Xu, and Jing (2014).

	Minimum	Maximum	Mean	Median
Free energy $E_f$ [ $10^{30}$ erg]	0.4	950	120±160	64
Dissipated magnetic energy $E_{diss}$ [ $10^{30}$ erg]	1.5	1500	180±250	110
Nonpotential magnetic field strength $B_{np}$ [G]	80	900	270±160	240
Free energy field strength $B_f = B_\varphi$ [G]	14	390	80±60	70
Length scale $L$ [Mm]	13	240	40±25	34
Electron density $n_e$ [ $10^{10}$ cm $^{-3}$ ]	3	56	10±7	9
Alfvén velocity $v_A$ [km s $^{-1}$ ]	380	8000	2100±1300	1700
Flare duration $\tau_f$ [s]	290	15,000	1500±1800	900

Table 2: Four versions of the Petschek model (MR1, MR2, MR3, MR4) applied to 162 M- and X-class flare events analyzed in Aschwanden, Xu, and Jing (2014). The results are given by the power exponent  $p$  of the scaling law, the energy ratio  $q_E = E_{diss}/E_{obs}$  (computed for an Alfvén Mach number of  $M_A = 0.1$ , and the cross-correlation coefficient  $CCC$  between the theoretically scaling law and observed energy values.

Model	Observed energy $E$	Alfvén velocity, $v_A$	Volume scaling $V$	Power exponent $p$	Energy ratio $q_E$	Cross-Correlation coefficient CCC
Petschek MR1	$E_{diss}$	$v_A = 1700$ km s $^{-1}$	$V = L^3$	1.35	0.68	0.79
Petschek MR2	$E_{diss}$	$v_A(B, n_e)$	$V = L^3$	1.52	0.64	0.73
Petschek MR3	$E_{diss}$	$v_A = 1700$ km s $^{-1}$	$V = L^2\lambda$	1.07	0.96	0.73
Petschek MR4	$E_{diss}$	$v_A(B, n_e)$	$V = L^2\lambda$	1.23	0.94	0.67



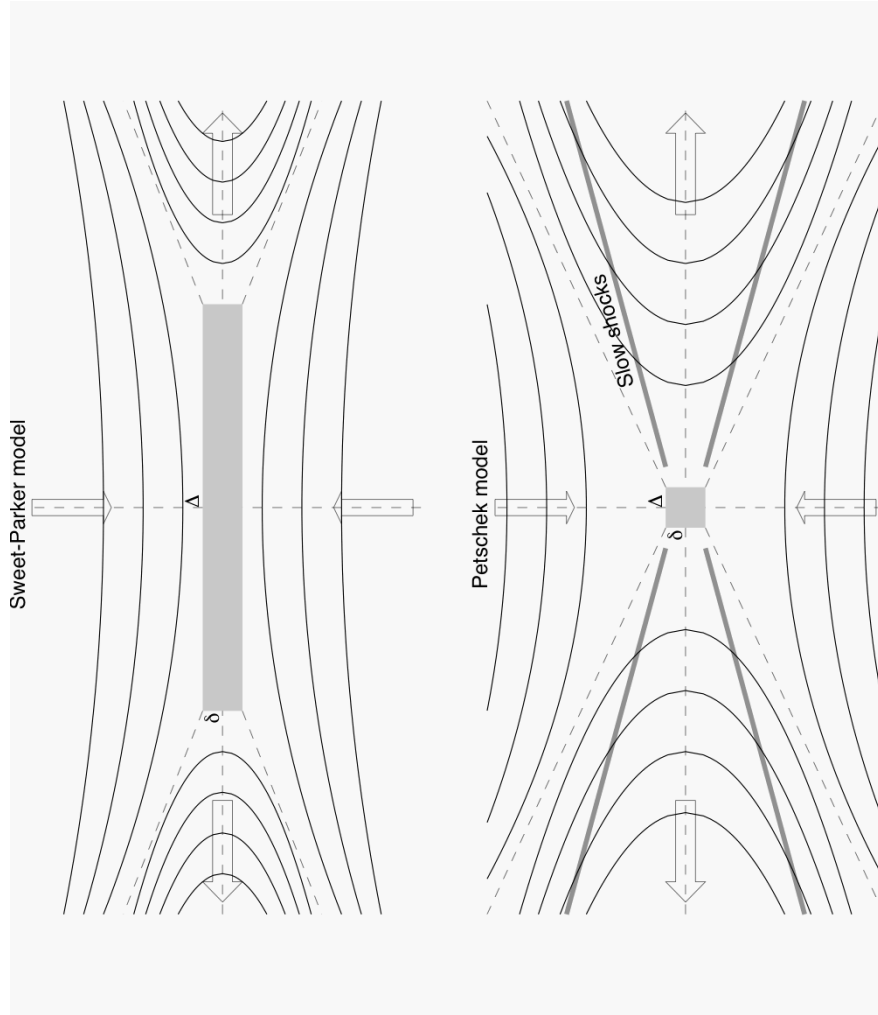


Fig. 1.— Geometry of the Sweet–Parker (top) and Petschek reconnection model (bottom). The geometry of the diffusion region (grey box) is a long thin sheet ( $\Delta \gg \delta$ ) in the Sweet–Parker model, but much more compact ( $\Delta \approx \delta$ ) in the Petschek model. The Petschek model also considers slow-mode MHD shocks in the outflow region.

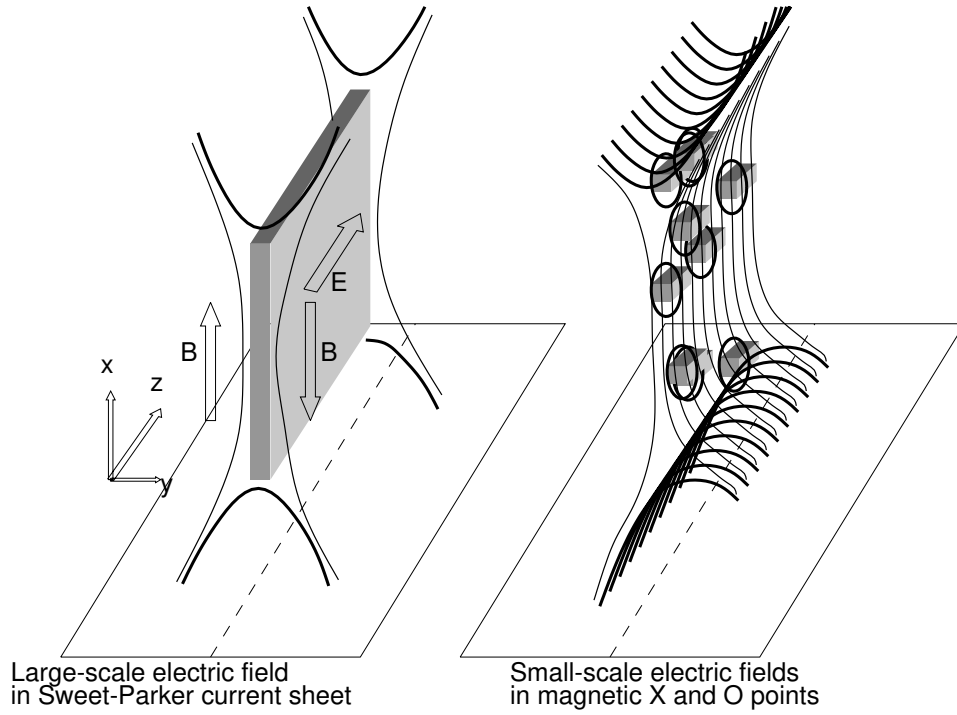


Fig. 2.— Paradigm shift of current sheet structure and associated particle acceleration regions: *Left*: classical models assume large-scale electric fields based on Sweet–Parker magnetic reconnection, which have a much larger extent in the  $x$  and  $z$ -direction than their width in the  $y$ -direction. *Right*: theory and MHD simulations, however, imply small-scale electric fields in magnetic X-points and coalescing islands with magnetic O-points (Aschwanden 2002).

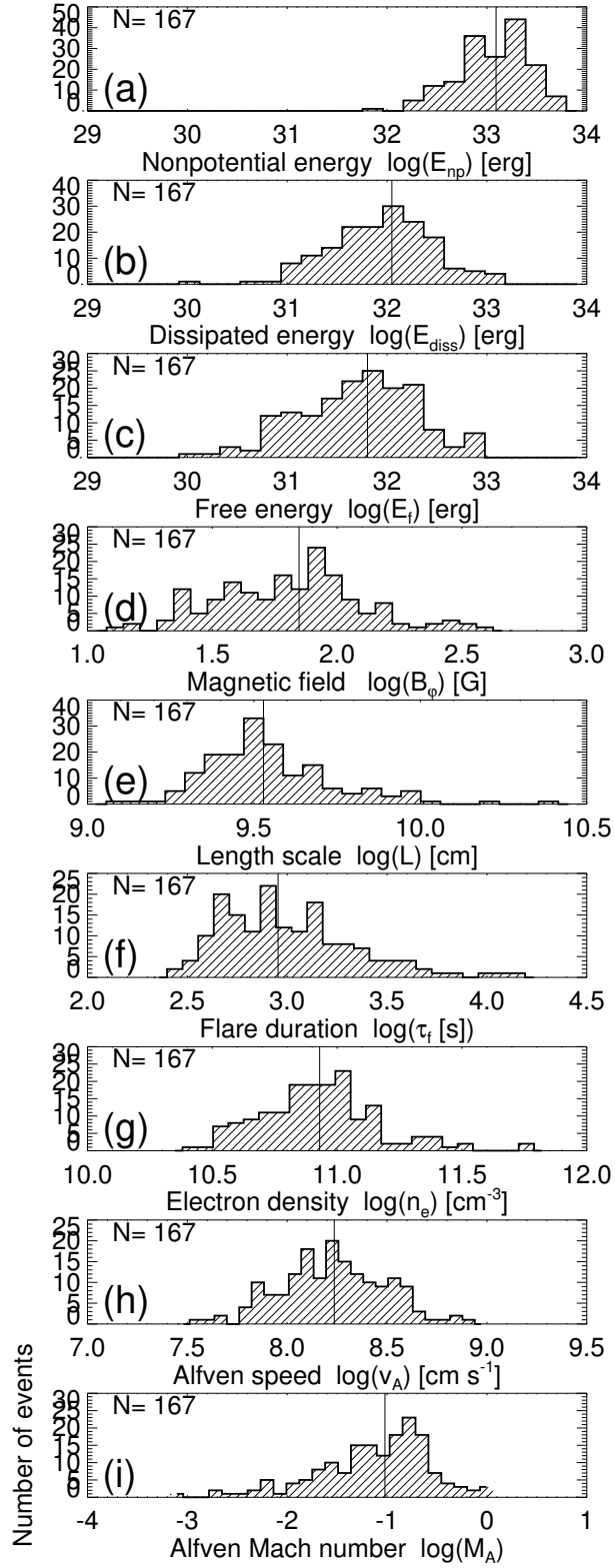


Fig. 3.— Histogrammed distributions of observables and derived physical parameters of 162 analyzed M- and X-class flare events. The median values are marked with a vertical line, see also Table 1.

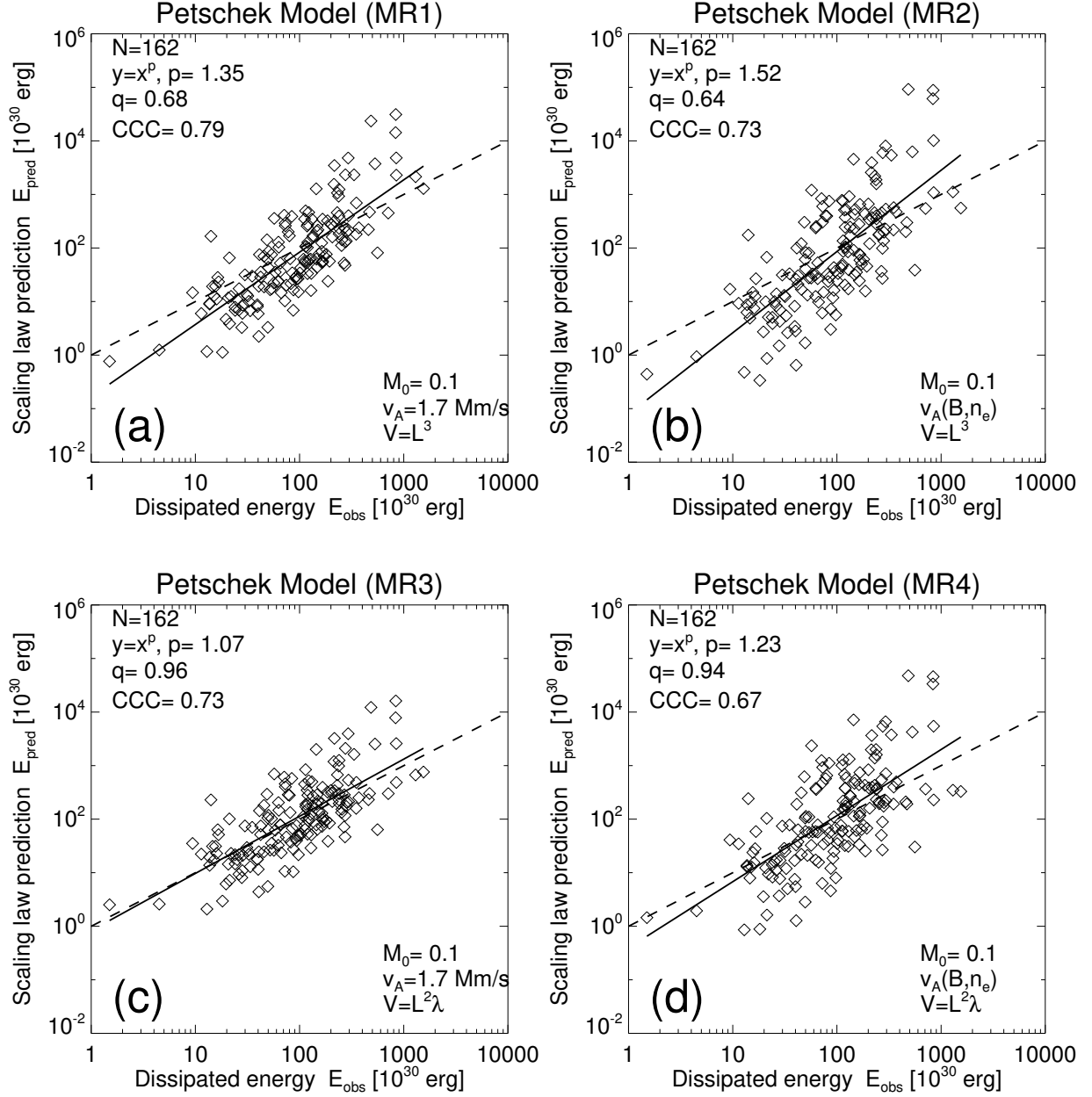


Fig. 4.— The scaling law prediction of four versions (MR1, MR2, MR3, MR4) of the Petschek model as a function of the observed dissipated energy  $E_{\text{diss}}$  from a set of  $N = 162$  M- and X-class flare events (diamond symbols). The four model versions embody different scalings of the Alfvén velocity ( $v_A = 1700 \text{ km s}^{-1}$  versus  $v_A(B, n_e)$ ), or volume scaling ( $V = L^3$  versus  $V^{2\lambda}$ ), and Mach number is  $M_A = M_0 = 0.1$ . The solid lines show linear regression fits, and the dashed lines represent equivalence between the observed dissipated energies and the predicted scaling law energies.

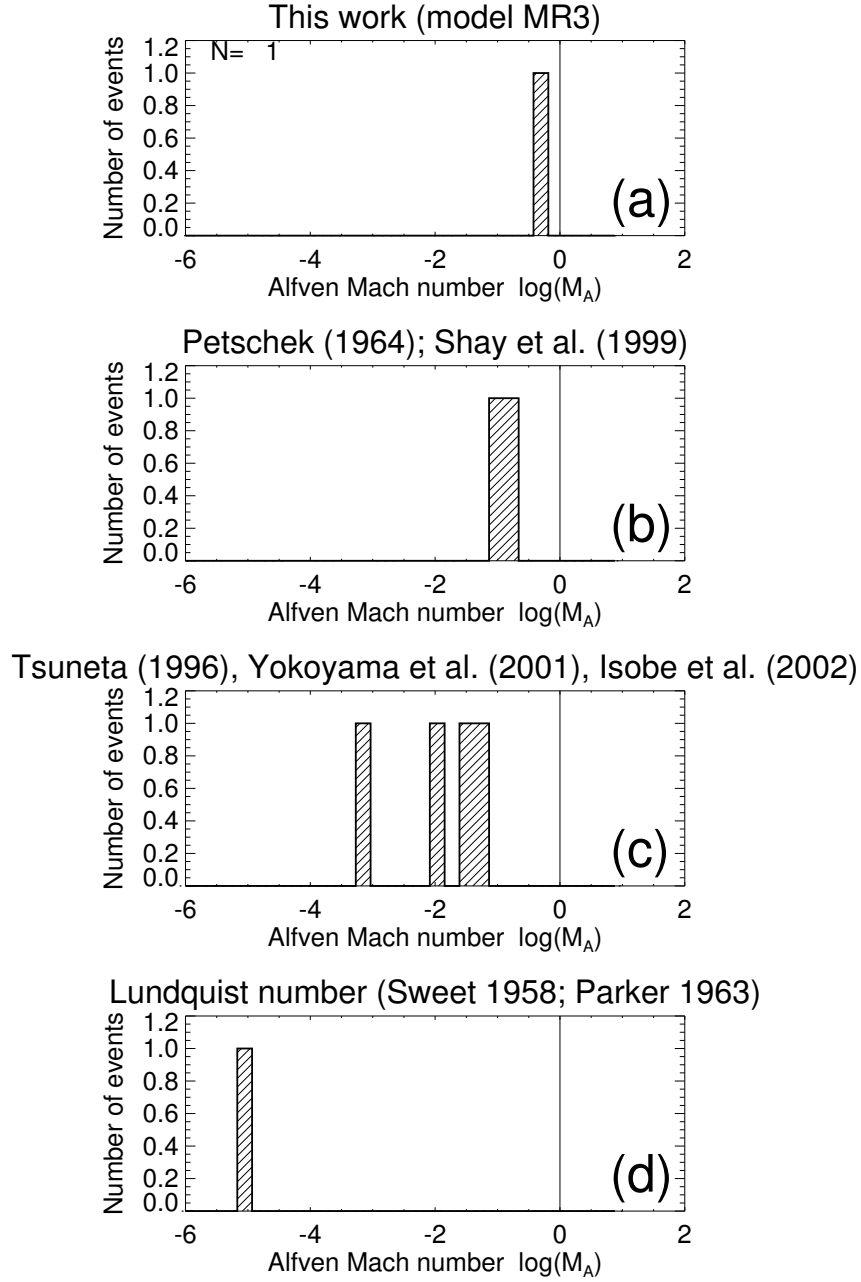


Fig. 5.— Theoretical (panels b and d) and observational estimates of the Alfvén Mach number  $M_A$ , derived from Yohkoh/SXT observations (c) and from model MR3 in this work (a).